JOURNAL OF GEOPHYSICAL RESEARCH, VOL. 104, NO. C5, PAGES 11,115–11,135, MAY 15, 1999

Numerical study of the circulation in a steep canyon off the Catalan coast (western Mediterranean)

Fabrice Ardhuin,[1,2,3] Jean-Michel Pinot,[2] and Joaquin Tintoré

Institut Mediterrani d'Estudis Avançats, Consejo Superior de Investigaciones Científicas-Universitat de les Illes Balears, Palma de Mallorca, Spain

Abstract. We use a limited-area fine-resolution primitive equation model to carry out a case study of the circulation in the steep and narrow Blanes Canyon, located off the Catalan coast (western Mediterranean). This area is characterized by a permanent along-slope density-driven current and strong northerly and easterly wind bursts in autumn. In a first step the slope current is allowed to adjust to the bottom topography, leading to a stationary circulation pattern which presents large vertical variations related to the canyon geometry. In the surface layer the strong stratification allows the current to flow straight over the canyon rim, ignoring bottom topography. In the intermediate layer the canyon is wide, and waters are isolated in a geostrophic anticyclonic eddy maintained by friction at the edge of the slope current. In the deep layer the canyon is narrow, and a topographic upwelling lifts bottom waters toward the canyon head. In a second step the circulation is forced by easterly (along-shore with the coast on its right) and northerly (seaward) 1-day wind bursts which induce significant vertical and cross-shore motions steered by the bottom slope. This ageostrophic circulation is substantially amplified in the canyon where the flow pattern presents large-amplitude oscillations characterized by a downwelling (upwelling) during the easterly (northerly) wind burst followed by a rebound upwelling (downwelling) as the wind relaxes. The upwelling induced by the northerly wind burst is capable of renewing waters trapped in the canyon eddy. Our results appear to be in fairly good agreement with in situ physical and biogeochemical data collected in Blanes Canyon and comparable canyons of the world ocean. The three-dimensional features obtained in this study can explain some of the observed patterns of larvae distribution and exchanges between the coastal zone and the open sea.

1. Introduction

Submarine canyons are characteristic features of many continental margins around the world. As is the case with other prominent topographic irregularities, they provide particular locations where a variety of ocean processes are reported to occur, fully three-dimensional, in general, because of the underlying uneven seabed (see *Hickey* [1995] for a review). A reasonable quantity of observational evidence, mostly in the geological and biological fields, shows that canyons are privileged places for the exchange of water between the coastal zone and the open ocean [e.g., *Church et al.*, 1984]. Coastal waters are generally confined to the continental shelf because of the presence of fronts at the shelf edge associated with energetic currents flowing along the isobaths, which represent true physical barriers to the offshore transport of properties. Canyons, by disrupting the mean along-slope flow pattern, seem to be capable of producing significant motions across the slope. This enhanced cross-slope transport of properties over canyons is of particular importance for the renewal of coastal polluted waters.

Canyons are not only significant because of the existing shelf-slope exchanges, but also because of the vertical motions steered by their steep topography and by the mesoscale eddies developing in their vicinity. Hence, vertical velocity is a key variable for the dynamics of canyon circulation. It is also a crucial parameter to study the interdisciplinary effects of the circulation since it determines the vertical exchange between nutrient-rich subsurface waters and the surface euphotic layer. The detailed description, from hydrographic and

[1]Visiting student from Ecole Polytechnique, Palaiseau, France.

[2]Now at Centre Militaire d'Océanographie, Etablissement Principal du Service Hydrographique et Océanographique de la Marine, Brest, France.

[3]Also at Department of Oceanography, Naval Postgraduate School, Monterey, California.

Paper number 1999JC900029.
0148-0227/99/1999JC900029$09.00

mooring data, of the three-dimensional circulation in Astoria Canyon (U.S. west coast) by *Hickey* [1997] also emphasizes the role of wind forcing in the amplification of these vertical motions in the canyon. She reports estimates of vertical velocity as large as 90 m day^{-1} inside the canyon.

Owing to the difficulties encountered in conducting systematic field experiments in canyons, the modeling approach is particularly relevant and has been used in the last years to get insight into the dynamics of canyon circulation [e.g., *Klinck*, 1996; *Allen*, 1996]. These studies provide a valuable contribution to our knowledge of canyon circulation by identifying the main physical factors at play in the adjustment between the flow, the density field, and the topography: stratification, alongshore flow direction with regard to the coast, nonlinearities, and wind. Their main shortcoming may be the representation of canyon topography by largely idealized shapes (uniform step, rectangle, Gaussian, etc.) which do not take into account the complexity and asymmetry of real bathymetry. These studies nevertheless paved the way for more realistic modeling experiments taking into account the particularities of one or another canyon. This is the case with *Petruncio* [1996], who observed and modeled a strong internal tidal signal in Monterey Bay Canyon. Our modeling experiments are part of this case-study effort, putting idealized results into a more complex and realistic perspective.

The objectives of our study are to model and analyze the flow in the area of Blanes Canyon, located off the northeastern Spanish (Catalan) coast in the western Mediterranean. This research is motivated by several observations collected in this particular canyon and other canyons of the Catalan slope [*Masó et al.*, 1990; *Álvarez et al.*, 1996; *Rojas et al.*, 1995], and also in canyons of other continental slopes (mainly the rich observations from Astoria Canyon [*Hickey*, 1997]) which evidence that specific processes take place in canyon areas: closed eddies, trapping of particles, enhanced ageostrophic motions, and puzzling larvae patterns. Probably the most general observation concerning the characteristics of the flow in canyons is the enhancement of the variability at these particular places. Available in situ data today, however, provide few hints about the nature of these processes, their forcing mechanisms, and their quantitative impact on the ecosystem. By carrying out this numerical work with an ocean circulation model, we hope to get some understanding about these crucial questions and obtain a concept of canyon circulation to help the interpretation of in situ data.

First, we focus on the stationary flow associated with the forcing by a constant along-slope current prescribed upstream of the canyon. Next, we investigate the transient adjustment associated with two different types of uniform winds that represent typical wind bursts observed off the Catalan coast in autumn. In the different experiments we pay special attention to the quantification of transports between the shelf and slope and to the description of water parcels displacements by means of Lagrangian trajectories. The structure of the paper is as follows. The canyon topography and mean flow characteristics are described in section 2. In section 3 we provide a description of the numerical model and its parameters together with the diagnostic tools used to analyze the model data. Results from the different simulations are described in sections 4 (no wind) and 5 (northerly and easterly wind bursts). Section 6 discusses the robustness of these results, on the basis of several sensitivity experiments, and their validity, on the basis of available observations. Finally, conclusions are provided in section 7.

2. Topography of Blanes Canyon and Mean Flow Characteristics

The continental margin in the Gulf of Lions and Catalan Sea is indented by a series of canyons which cut across the slope (Figure 1). Blanes Canyon, located off the Catalan coast, is one of the most prominent of these canyons. In this area the shelf is narrow and the shelf-break ($\sim$ 200 m) is found at 20 or 30 km from the coast. The canyon rim lies at 100 m, where it interrupts the shelf. At this depth the head of the canyon is only 5 km away from the coast. Close to the coast, the canyon narrows with depth down to 900 m, and it is particularly steep: The maximum slope of its flanks is 40%, while the average slope of the shelf-break outside the canyon is 5%. At 800-m depth the width of the canyon head is less than 3 km. At the mouth, located 40 km offshore, the canyon is about 12 km wide, and its bottom declines more gently down to the offshore seabed at 1800-m depth.

A permanent energetic current is found over the Catalan slope, flowing southward in a direction almost perpendicular to the canyon axis. It belongs to the large-scale current which circulates along the northern slope of the western Mediterranean, with the coast on its right [*Millot*, 1987]. This mean circulation is clearly seen in satellite images of sea surface temperature for it advects a tongue of surface fresh and cold continental waters originated from the Rhône River in the north [*La Violette et al.*, 1990]. The current is strongly baroclinic, in almost geostrophic balance with a marked density front due to the salinity contrast between relatively fresh coastal waters and more saline offshore waters. Stratification largely depends on the season. The mean stratification is characterized by a bouyancy frequency N close to $4 \times 10^{-3}\,\mathrm{s}^{-1}$. In summer, stratification reaches its highest value in the upper 100 m, strongly heated by the Sun. However, the largest transport values ($\sim$ 2 Sv) are measured in winter when the flow is more barotropic, while it is in the range 1-1.5 Sv in summer [*Font et al.*, 1988; *García-Ladona et al.*, 1996]. Over the shelf the circulation is weak and variable, mostly driven by instabilities developing at the onshore edge of the slope current and transient winds.

The characteristics of the current core, bounded by

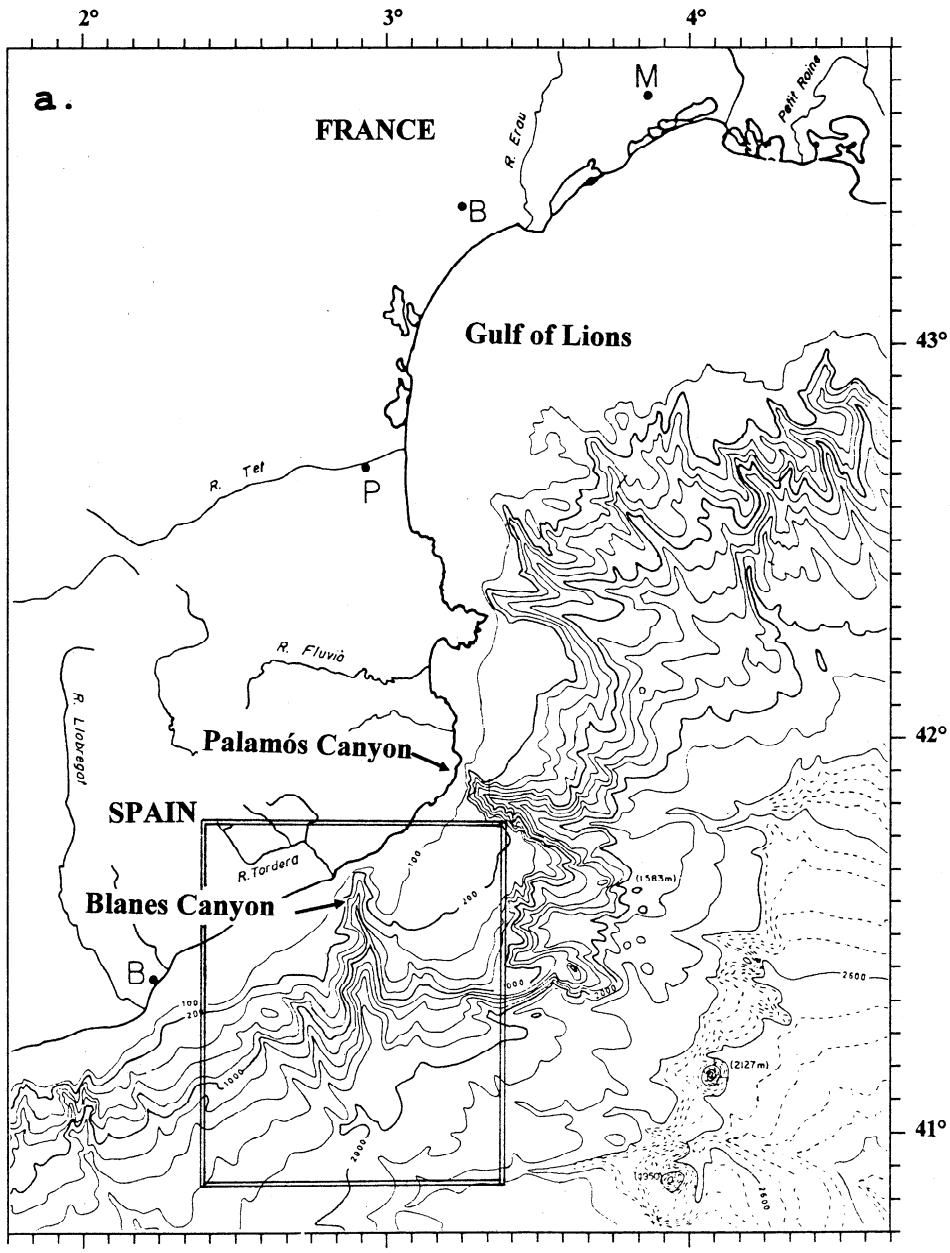

Figure 1. (a) Topography of the northwestern Mediterranean and (b) magnified view in the area of Blanes Canyon. Adapted from *Canals et al.* [1982].

the 5 cm s^{-1} isotach, are $l = 30$ km for width, $d = 300$ m for depth, and $U = 30$ cm s^{-1} for surface velocity [see, e.g., *García-Ladona et al.*, 1996]. Outside the core the background flow is typically a few centimeters per second. Hence, for the mean flow incident on the canyon the Rossby number ($Ro = U/fl$) is about 0.1 at the surface (the Coriolis parameter f is taken at 41.5 N). The mean bouyancy frequency N gives an internal Rossby radius of deformation ($R_d = Nd/f$) equal to 13 km. Thus the canyon is twice as deep as the incident flow, and its width is of the order of the internal Rossby radius of deformation. Following definitions by *Hickey* [1997], Blanes Canyon can be considered as fairly deep and moderately narrow, except between 200 and 500 m, where it significantly narrows.

The area of Blanes Canyon is particularly well suited for the study of the interaction between a density-driven flow and complex topography. Winds are generally weak, except for strong northerly and easterly wind bursts in autumn, and tidal currents are negligible. Several hydrographic cruises have been carried out in the area to investigate the role of the canyon in modifying the slope circulation and enhancing cross-slope exchanges. In particular, *Álvarez et al.* [1996] showed significant cross-shore displacements of the slope current axis, shifting from 10 to 30 km from the coast upstream of Blanes Canyon on a timescale of 10 days.

3. Numerical Model

The model we use for our simulations is based on a numerical code developed by *Wang* [1982]. It is

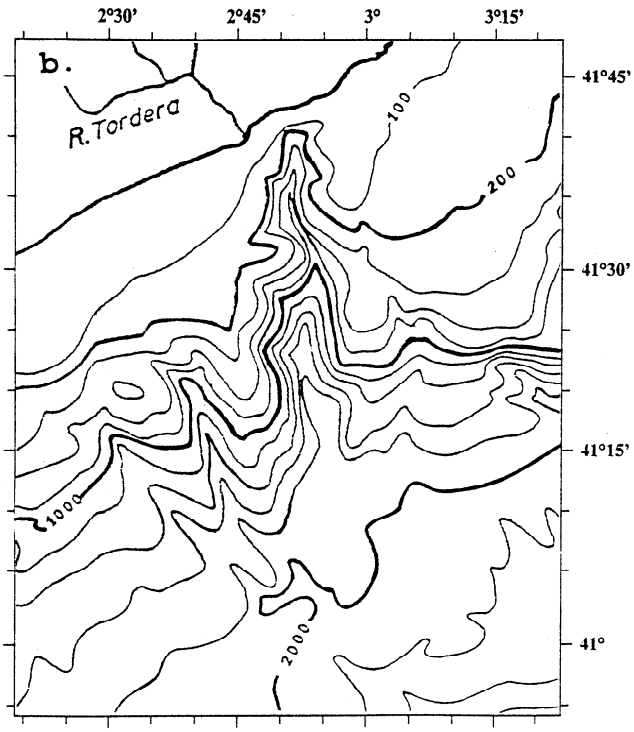

Figure 1. (continued)

a regional free-surface three-dimensional coastal ocean model which solves the primitive equations in Cartesian coordinates with a z coordinate in the vertical. Details of the model formulation are not reproduced here, but they are given by *Wang* [1982, 1997].

3.1. Model Parameters

At the coast the model uses a free-slip boundary condition and zero normal momentum flux. A quadratic law is used for bottom friction with a drag coefficient C_B set to 3×10^{-3}, and bottom vertical velocity is set to zero.

In the momentum equation, eddy viscosity is second order with a constant coefficient in the horizontal, ν_H, set to 10 $m^2 s^{-1}$. In the vertical, it is flow dependent according to the parameterization by *Munk and Anderson* [1948]:

$$\nu_z = 10^{-3} + 10^{-2}(1 + 10R_i)^{-1/2} \ m^2 s^{-1} \qquad (1)$$

where R_i is the Richardson number.

In the density equation the diffusivity is also second order with a coefficient in the horizontal, K_H, set to 10 $m^2 s^{-1}$. In the vertical we use Smagorinski's parameterization:

$$K_z = 50(1 + 3.33R_i)^{-3/2} \ m^2 s^{-1} \qquad (2)$$

The model area is shown in Figure 2. Velocity components u (cross-shore), v (along-shore), and w (vertical) are counted positive pointing offshore (x axis), upstream (y axis), and upward (z axis), respectively. Boundaries are open upstream, downstream and offshore. Except for v, which is prescribed at the upstream boundary in order to model the observed inflow, we use an Orlanski radiation condition both upstream and downstream, which allows flow perturbations to exit the domain [*Orlanski*, 1976; *Wang*, 1997]. At the offshore boundary the cross-shore transport is set to zero, while surface elevation and baroclinic flow components are kept gradient-free, which lets the Ekman transport go through the boundary. However, open boundaries are placed far enough from the canyon to avoid contamination by spurious boundary effects. The upstream boundary condition is placed 60 km upstream of the canyon to allow the geostrophic inflow to adjust to the bottom slope before reaching the canyon.

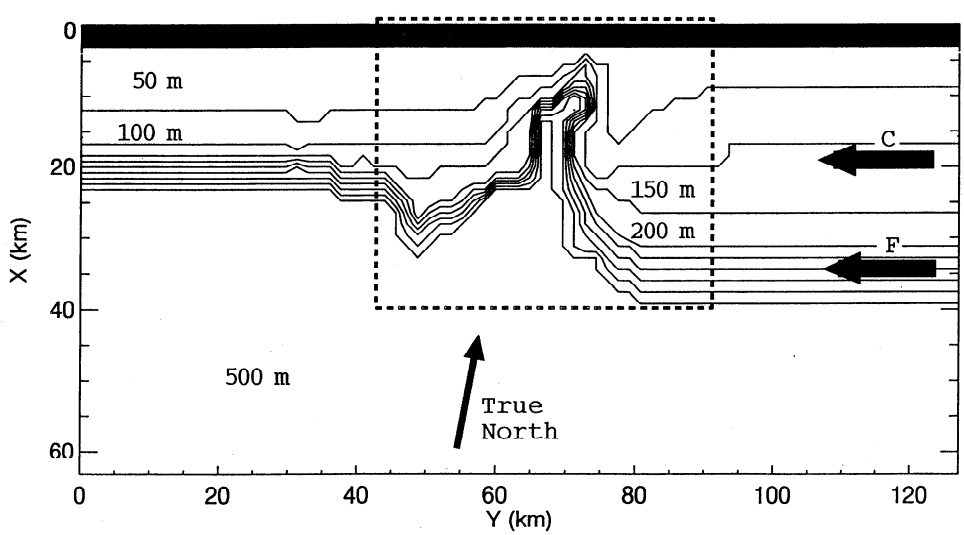

Figure 2. Representation of bottom topography in the model domain. The x axis points offshore almost to the south and the y axis points upstream to the east. Isobaths between 50 and 500 m are plotted every 50 m. Along-shore arrows indicate the location and direction of the current core at the upstream boundary in configuration SH (current core over the shelf) and SL (current core over the slope). The dashed box indicates the zoom window used in Figure 5 and following.

Bottom topography is derived from *Canals et al.* [1982]. Horizontal resolution in the model is set to 1.6 km. In the vertical we use 10 levels, each 50 m thick. Time steps are 5 s and 100 s for the external and internal mode, respectively. Since the study is focused on the interaction of the energetic core of the flow (upper 300 m) with the canyon, we restrict the model to the part of the canyon which is closest to the coast by placing the bottom at 500 m, that is, 200 m beneath the core of the current, and at the average depth of the head of the canyon. Besides, the circulation inferred from hydrographic data [*Álvarez et al.*, 1996] on the slope is weak below 500 m; we therefore assume that it does not significantly influence the upper flow pattern. This point is discussed in more detail in section 6.1. The limit on the bottom depth saves computing time by reducing the number of levels and by increasing the time step of the external mode.

3.2. Density and Atmospheric Forcings

For model initialization a density field s is imposed in all the model domain, representing a surface-intensified cross-shore front uniform in the along-shore direction. It is modeled by the following mathematical expression:

$$s = s_0 - \frac{\Delta s_0}{2}\left[1 - \tanh\left(\frac{x - x_0}{w_0}\right)\right]\exp\left(\frac{-z}{h_0}\right) \quad (3)$$

where s_0 is a homogeneous background density, Δs_0 represents the across-front density contrast, x_0 is the distance of the front from the coast, w_0 is the scale of the front width, and h_0 is the scale for the density change with depth, which controls stratification. Note that there is no stratification offshore where density is almost homogeneous and tends towards s_0.

The associated geostrophic flow field is calculated in the first time step with reference to the bottom at 500 m without taking into account the bottom topography. A barotropic component of 3 cm s^{-1} is added to include a weak along-slope flow at depth. Both density and geostrophic velocity are maintained constant at the upstream boundary during all simulations.

We use two flow configurations (Figure 3) on the basis of the observations described by *Álvarez et al.* [1996]: a configuration where the along-slope flow is centered over the shelf (configuration "SH," for shelf), and a configuration where the flow is centered further offshore over the slope (configuration "SL," for slope). All parameters appearing in (3) are given in Table 1 for both configurations. They are tuned to reproduce the characteristics of the observed density and current fields.

The first experiments are done without considering any wind forcing and exclusively aim at establishing the patterns of the steady circulation (they are labeled as experiments "S," for steady). Two other sets of experiments are carried out which consider the effect of the easterly and northerly wind bursts prevailing in autumn (these experiments are labeled as "WE" and "WN," respectively). In both cases a constant forcing is applied during 1 day to the steady circulation obtained in experiment S, followed by 9 days of calm. The wind forcing is also uniform in space (aligned with the y axis and x axis in experiments WE and WN, respectively, and therefore either purely along-shore or cross-shore) since the size of the study area is small compared to the scale of the meteorological mesoscale forcing. The wind strength is represented by a surface stress 0.32 Pa which corresponds roughly to a wind of 10 m s^{-1} blowing 10 m over the sea surface.

3.3. Model Diagnostic: Volume Transports and Lagrangian Trajectories

To measure the balance between along-shore, cross-shore, and vertical fluxes, volume transports are computed in each layer by integrating velocity at the sides of a closed box encompassing the canyon ("canyon box" in Figure 4). The dimensions of this box are 19 km along-shore and 12 km cross-shore. The along-shore side intersects the canyon and shrinks to 3.2 km at the bottom. Fluxes are also computed in a similar box located upstream of the canyon ("upstream box" in Figure 4) in order to better assess the role of the canyon in modifying the fluxes by comparison to a straight portion of the slope. At the offshore side of the boxes we reckon the net cross-shore fluxes U_i in the different layers and the total onshore fluxes $U^-_{\rm tot}$ and offshore ($U^+_{\rm tot}$) fluxes integrated from surface to bottom. The vertical fluxes (W_i) between model layers are computed too. All fluxes are expressed as a ratio (in percentage) to the total along-slope inflow $V_{\rm tot}$, the sum of $V_{\rm shelf}$ and $V_{\rm slope}$ upstream of the canyon (Figure 4).

Three-dimensional Lagrangian trajectories of neutrally bouyant drifters (representing water parcels or, equivalently, a passive particulate tracer in suspension) are calculated to provide a complementary view to the model Eulerian dynamics. The error on the particle displacement is reduced by using a first-order predictor-corrector scheme [*Press et al.*, 1992]. At each time step (100 s) a first guess of the final position of the particle is estimated from the velocity at the initial position. Then, both positions are used to calculate a mean velocity along the path of the particle and to recalculate the final position. To interpolate velocity components from the model mesh to the particle position, we use a triangular weight function derived from *Monhagan* [1985]. The footprint of this weight function covers three points of the Eulerian grid along each axis. This guarantees the representativity of the trajectories.

4. Steady Adjustment to Topography (Experiments S)

The model is initialized with the density and geostrophic velocity fields described in section 3.2. These fields are prescribed at the upstream boundary during the whole simulation and represent the only forcing to the

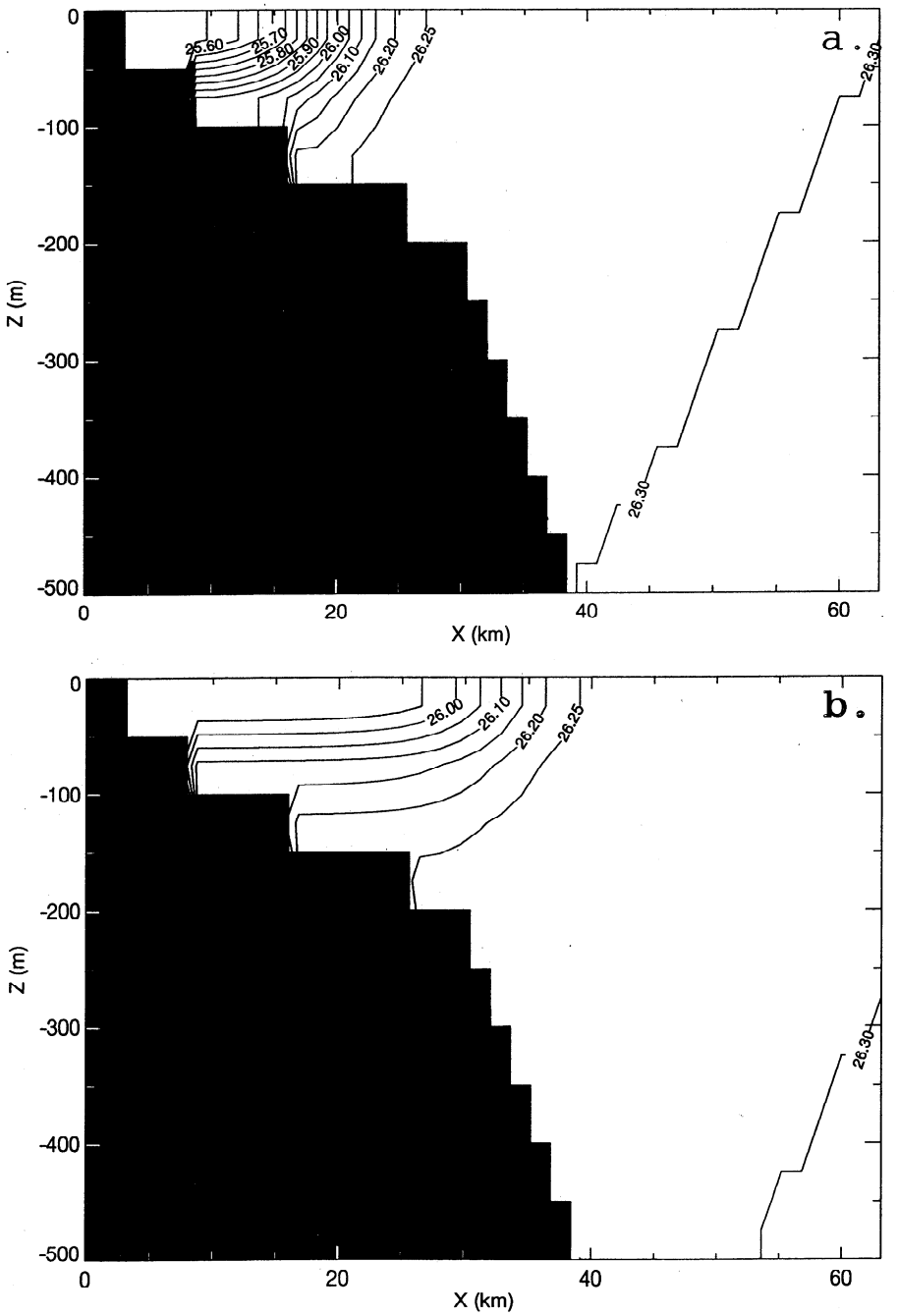

Figure 3. Cross-shore vertical structure of the density front and associated geostrophic inflow prescribed at the upstream boundary: density (in σ_t units) in configurations (a) SH and (b) SL and geostrophic velocity (in $\mathrm{cm\,s^{-1}}$) in configurations (c) SH and (d) SL.

circulation. Two experiments are carried out, S-SH and S-SL, using the configurations described in Table 1. After 7 days the flow is almost adjusted to the bottom topography, but we let the model run up to 50 days to ensure that the circulation reaches a steady state. This duration is enough for the deepest waters generated at the upstream boundary to be advected through the model domain (mean bottom velocity is $\sim 3\ \mathrm{cm\,s^{-1}}$) and reach the downstream boundary. After 50 days a cluster of Langragian drifters is released in the canyon, in a cross-shore vertical plane ($y_0 = 69$ km), and the simulation is pursued during another 40 days to compute their trajectories.

In experiment S-SH the current initially located over the outer shelf stabilizes slightly offshore over the shelf-break (Figure 5). Interesting results are obtained within the canyon where the flow pattern is characterized by strong vertical variations. In the upper 50 m the current flows straight over the canyon except a very small shoreward deflection over the rim of the canyon head (Figure 5a). The surface flow does not feel bottom topography because of the strong stratification in the

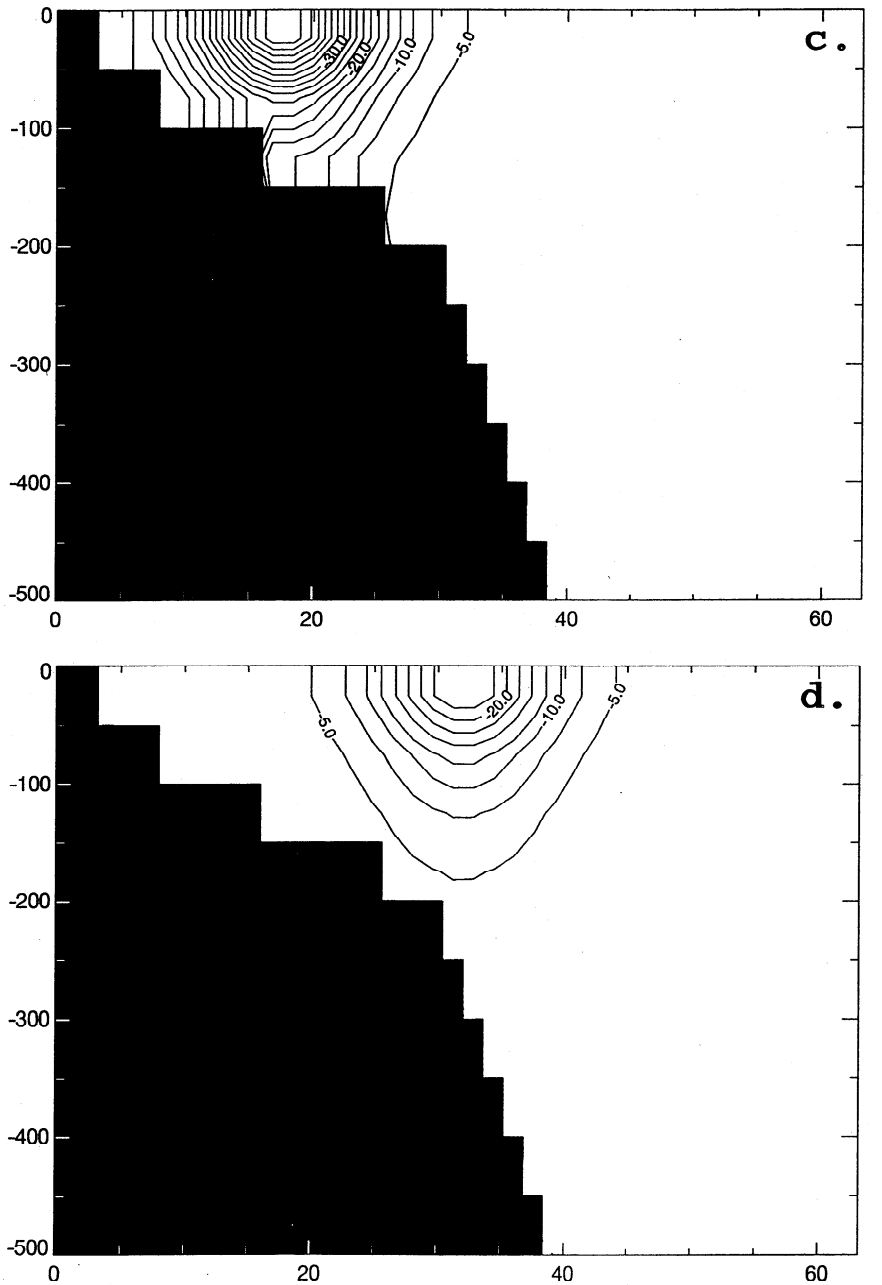

Figure 3. (continued)

upper layers (Figure 3b), which has a screening effect. At 75 m the flow is deflected seaward, driven by a submarine promontory at the upstream wall of the canyon (Figure 5b). Inside the canyon, in the lee of this promontory, a weak anticyclonic circulation develops with velocities of 1-3 $\mathrm{cm\,s^{-1}}$. At greater depths, between 100 and 200 m, this promontory is still present, and it shelters canyon waters which recirculate within a well-formed anticyclonic eddy (Figure 5c). The maximum anticyclonic relative vorticity in this eddy is about $0.2f$ at 125 m. Between 200 m and the bottom the canyon head drastically narrows, but its mouth widely opens offshore (Figure 5d). The along-slope flow turns slightly onshore as it passes by the canyon mouth and part of its waters impinge onto the downstream wall where they separate. The branch deflected onshore drives slope waters into the canyon. This onshore flow along the canyon axis is of the order of 1 $\mathrm{cm\,s^{-1}}$ at 375-m depth (Figure 5d).

Lagrangian trajectories clarify some aspects of this circulation (Figure 6). Among the drifters released in the canyon, all those which are initially located between 100- and 175-m depth follow closed trajectories (e.g., subset 1 in Figure 6a), confirming that the eddy is a closed recirculating pattern within which water parcels are trapped. Rotation speeds are, however, fairly weak, about 2-3 $\mathrm{cm\,s^{-1}}$, and the timescale is of the order of 10 days for a water parcel to complete one rotation within the eddy. Trajectories also reveal an upwelling cell beneath the eddy (Figure 6b). This cell is almost

Table 1. Parameters Defining the Prescribed Along-Slope Density Front and Associated Inflow at the Upstream Boundary in configurations SH and SL

Model Parameters	Configuration SH	Configuration SL
Maximum density at surface s_0, σ_t units	26.3	26.3
Across-front density contrast at surface Δs_0, σ_t units	0.8	0.4
Distance of the front axis from the coast x_0, km	15	30
Front width scale w_0, km	6.4	6.4
Front depth scale h_0, m	65	150
Along-shore total transport, Sv	1.02	0.83
Surface bouyancy frequency N, $10^{-3}s^{-1}$	7.7	3.6

confined to a vertical plane between the canyon walls. Offshore deep waters of the 300- to 500-m layer are lifted at the canyon wall and pulled back out to the open sea in the 200- to 300-m layer. This circulation is slow as drifters go up this cell in about 30 days. This vertical motion evidenced by trajectories is a topographic upwelling directly related to the onshore flow observed in lower layers (Figure 5d). As waters make their way toward the canyon head crossing isobaths, they are lifted over the bottom slope.

A detailed analysis of the along-shore momentum budget, at the mouth of the canyon and 125-m depth, shows that the horizontal eddy viscosity term has an antisymmetric dipole shape at the mouth of the canyon (not shown). The negative lobe lies in the canyon, where the flow at the offshore edge of the canyon eddy ($v < 0$) is accelerated westward, while the positive lobe is confined to the edge of the along-shore current, just outside the canyon, where the flow loses momentum. Nevertheless, the pressure gradient is still about 80% of the Coriolis force (both are 10 times smaller at 125 m than at 25 and 75 m), the diffusion in the cross-shore direction is about 13%, and the advection accounts for the remaining 7%. At the same depth but at the head of the canyon, where the flow is the direction opposite to the flow at the mouth, diffusion is negligible, and the Coriolis force is balanced by the pressure gradient (65%) and advection (35%).

In the cross-shore direction and on the canyon axis the pressure gradient balances over 95% of the Corio-

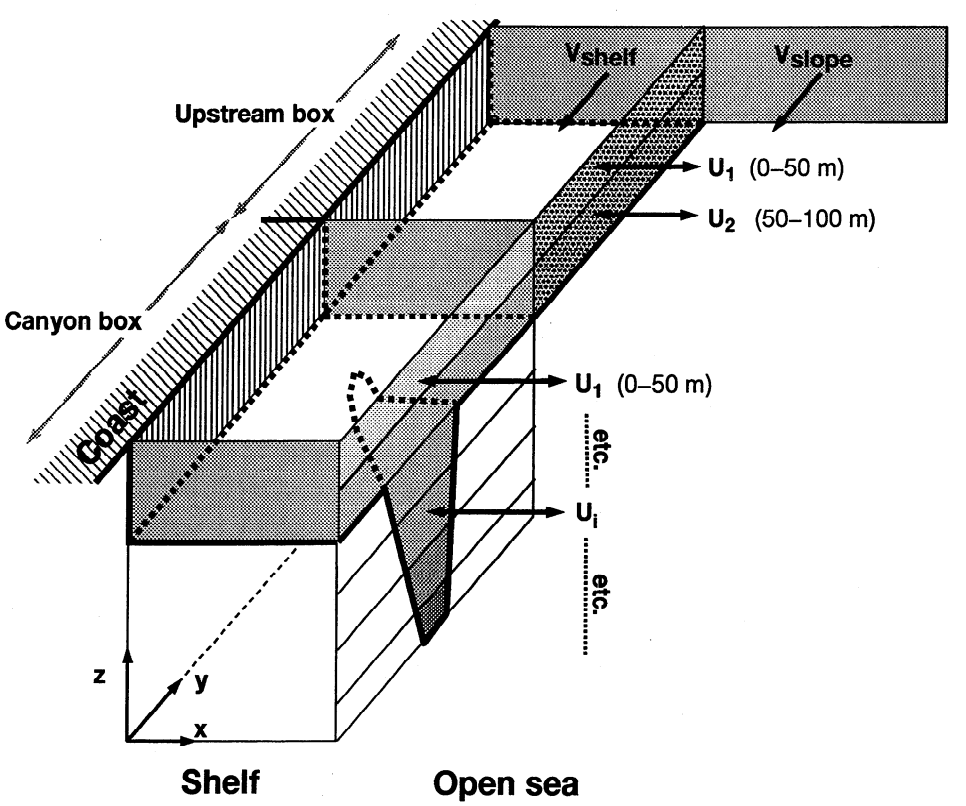

Figure 4. Schematic representation of the fluxes computed in the canyon ("canyon box") and over a straight portion of the slope ("upstream box"). U_1 to U_{10} are the net cross-shore fluxes through the offshore side of the boxes in layers 1-10. V_{shelf} and V_{slope} are the total along-slope transport upstream of the canyon over the shelf and the slope, respectively.

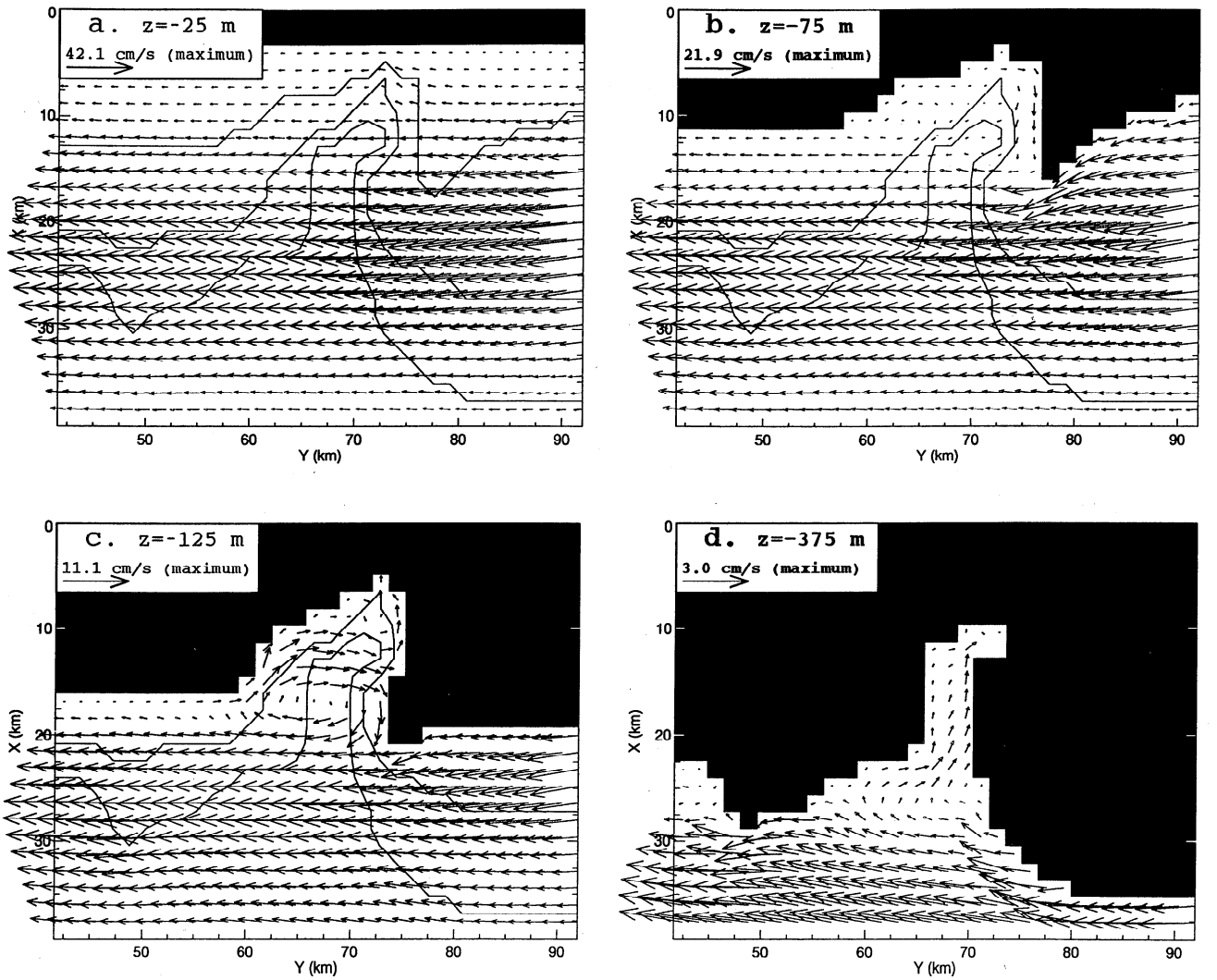

Figure 5. Steady circulation (experiment S-SH): Maps of horizontal velocity in the canyon at four representative depths 50 days after initialization. The 100-, 200-, and 400-m isobaths are plotted with solid lines.

lis force from the surface to 125 m, with a reversal of both terms at 125 m in the canyon head. This reversed pressure gradient, which is in the direction opposite to the one at the mouth of the canyon, is set by denser waters upwelled at the canyon head as confirmed by upward tilting trajectories (which are roughly isopycnal) toward the canyon head (Figure 6b). The flow field at 125 m (Figure 5c) corroborates that the eddy-induced westward flow impinging onto the downstream canyon wall produces a divergence and an onshore acceleration of the flow. Our interpretation is that eddy viscosity is responsible for the acceleration of the canyon waters in the along-shore direction at the mouth, and thus it is necessary for the generation and maintenance of the steady anticyclonic canyon eddy. This flow is in approximate geostrophic balance with a doming of the isopycnals at intermediate depth. This feature is also linked to the underlying upwelling cell, although we hold the latter to be a secondary effect. The vertical cell may also contribute to accelerate the base of the eddy by compressing isopycnals and generating anticyclonic vorticity.

In the cross-shore momentum budget, again, but below 200 m, geostrophy is weaker. Although the pressure gradient is much reduced from 125 m to the bottom, the imbalance at 175 m (which is about 30%) is enough to force offshore and onshore advection of waters, driving the vertical cell. This ageostrophic flow is made possible by the increase of the Rossby number although velocity weakens, as the along-canyon Coriolis acceleration vanishes along the walls. The flow is thus driven offshore, at intermediate depth and near the mouth of the canyon, by the unbalanced part of the pressure gradient. This effect is most conspicuous at the base of the stratified upper layer, at about 225 m depth (Figure 6b), where the canyon is sufficiently narrow (4.8 km). As the pressure gradient decreases with depth, this offshore flow diminishes and an onshore return flow is allowed by advection at the bottom, which feeds the vertical cell to ensure continuity.

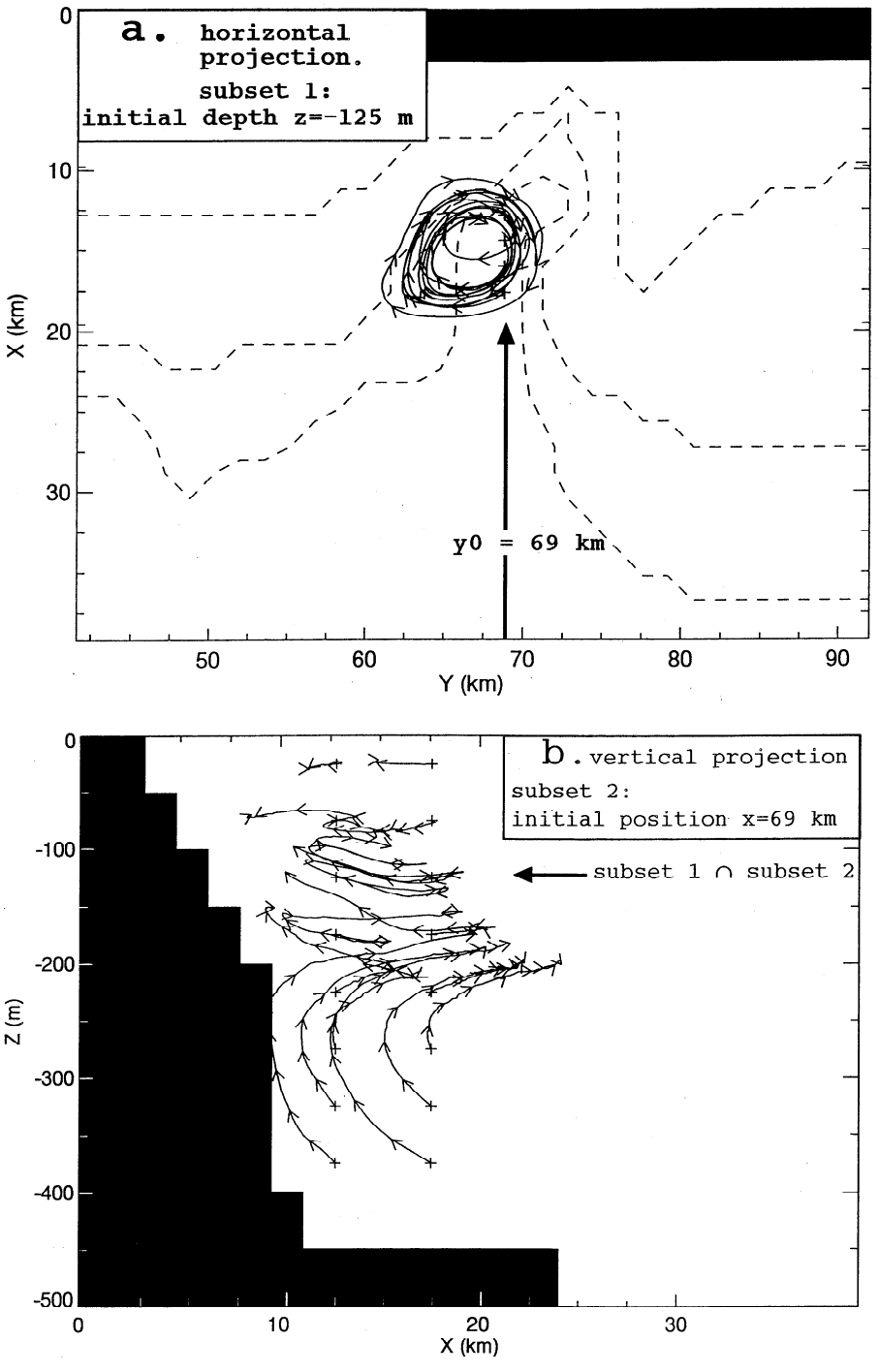

Figure 6. Steady circulation (experiment S-SH): trajectories of the drifters released 50 days after initialization at $y_0 = 69$ km within the canyon. The initial positions are represented by crosses, and arrows are plotted every 2 days to show the direction of the movement. (a) Horizontal projection of the 40-day trajectories of all drifters released at 125 m depth (subset 1). Bottom topography is indicated with dashed lines. (b) Vertical projection in a cross-shore plane (looking upstream) of the initial 16-day portions of a sample of trajectories (subset 2).

The volume transport in the cross-shore direction at the mouth of the canyon is very small in this experiment, with maximum values of about 0.02 and 0.01 Sv for the onshore fluxes $U^-_{\rm tot}$ and offshore fluxes $U^+_{\rm tot}$, respectively. These fluxes represent about 2% and 1%, respectively, of the total along-slope transport $V_{\rm tot}$, which is 1.0 Sv in configuration SH.

Results from experiment S-SL are similar to those described above for experiment S-SH, suggesting that circulation patterns have little sensitivity to the offshore location of the slope current. Nonetheless, velocities within the canyon tend to be lower in experiment S-SL because of the fact that the current core is located farther offshore, preventing the flow from interacting so

energetically with the bottom topography. In particular, the anticyclonic eddy forms slightly offshore, closer to the mouth of the canyon. The maximum anticyclonic relative vorticity is $0.1f$ in the eddy, which is half the value obtained in experiment S-SH, without any perceptible doming of the isopycnals. Likewise, velocities are weaker in the vertical cell.

5. Wind Forced Experiments

5.1. Response to an Easterly Wind Burst (Experiments WE)

The wind forcing (see section 3.2) is applied during 1 day to the 50-day steady circulation. This easterly wind blows with the coast on its right along the y axis. After wind relaxation the model is run for another 9 days in order to analyze the readjustment of the circulation and compute Lagrangian trajectories. Configurations SH and SL (Table 1) are investigated in experiments WE-SH and WE-SL, respectively. Results from experiment WE-SL are described in detail below, while results of WE-SH are used to discuss the sensitivity of the model to the offshore location of the current axis.

The wind forcing produces an oscillation of the flow characterized by an intense downwelling phase during the wind burst followed by upwelling as the wind relaxes. The downwelling velocities reach a maximum 12 hours after the outbreak of the wind. At this time the Ekman transport in the upper layer is directed onshore, producing a convergence in the coastal boundary layer (Figure 7a). This convergence leads to the formation of a narrow coastal jet that is particularly enhanced at the canyon head, where maximum currents are observed (~ 31 cm s^{-1}). Offshore waters entrained over the upstream flank of the canyon are pushed against the coast and further advected onto the inner shelf downstream of the canyon, forming this narrow coastal jet. This enhanced surface convergence at the canyon head is associated with a strong downwelling along the canyon axis and a return flow directed offshore in subsurface layers and generally enhanced at the downstream flank of the canyon (Figures 7b and 7c). This offshore flow is also produced to a lesser extent near the slope out-

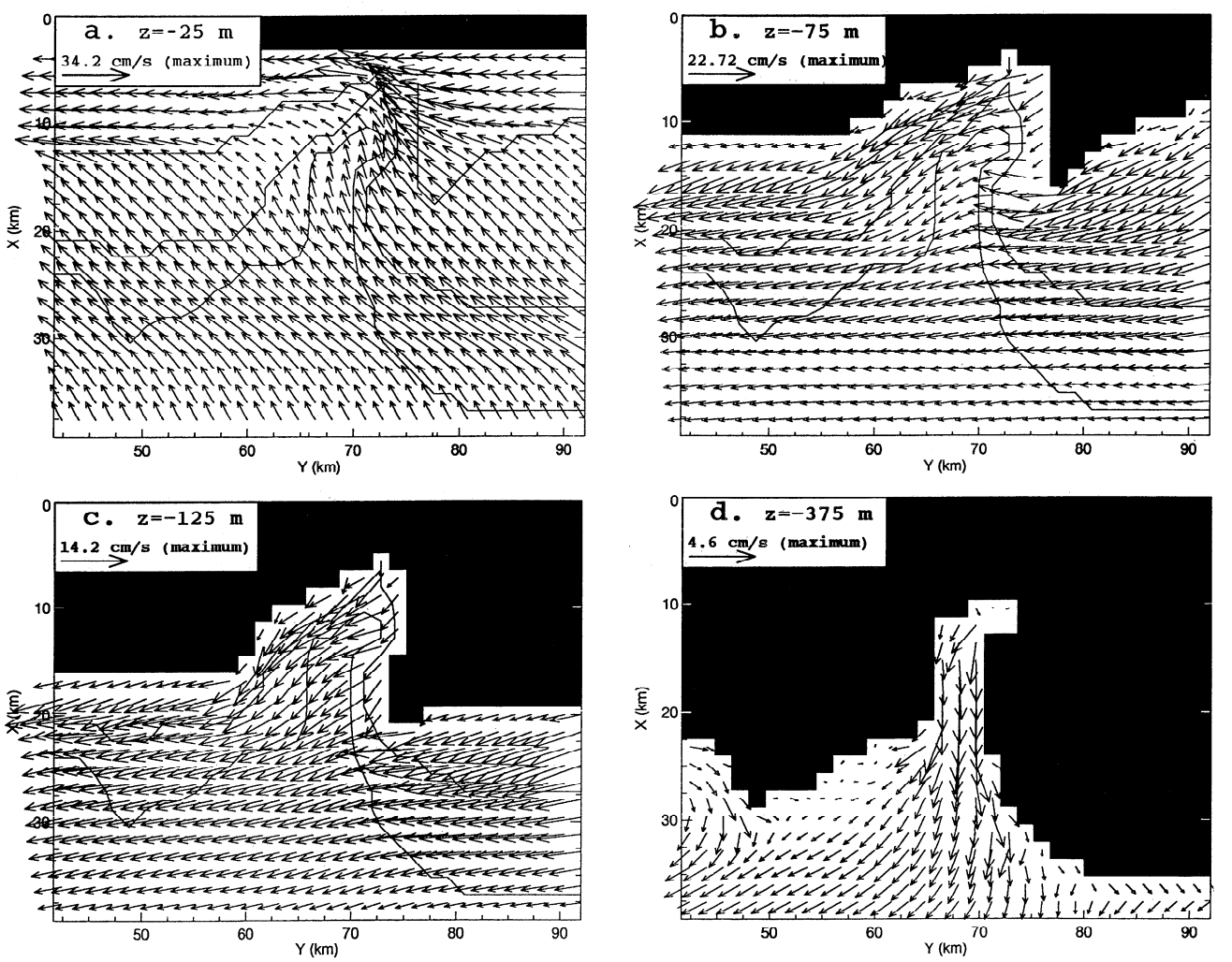

Figure 7. Circulation induced by an easterly wind burst (experiment WE-SL): maps of horizontal velocity in the canyon at four representative depths 12 hours after the wind starts. The 100-, 200-, and 400-m isobaths are plotted with solid lines.

side the canyon. The steady anticyclonic eddy located in the 100- to 200-m layer previous to the wind burst is completely disrupted by the energetic wind-induced flow ($\sim$ 10 cm s^{-1} at 125 m). In the deep layers the flow is funneled by the canyon walls toward the open sea (Figure 7d). However, velocities are weak at these depths ($\sim$ 3 cm s^{-1} at 375 m).

The time evolution of the flow response in the canyon is illustrated by a time series of the fluxes in the canyon box (Figure 8 and Table 2). As expected, inertial oscillations (the inertial period is 18.1 hours in the canyon area) are important during the wind burst, and they slowly decrease during the following days (see Figure 8a, where they have not been filtered out). The viscosity used in the model is quite low, and, accordingly, the damping of inertial oscillations, which do not propagate away because their group velocity is almost zero, is slow and can take as much as 10 days [*Tintoré et al.*, 1995].

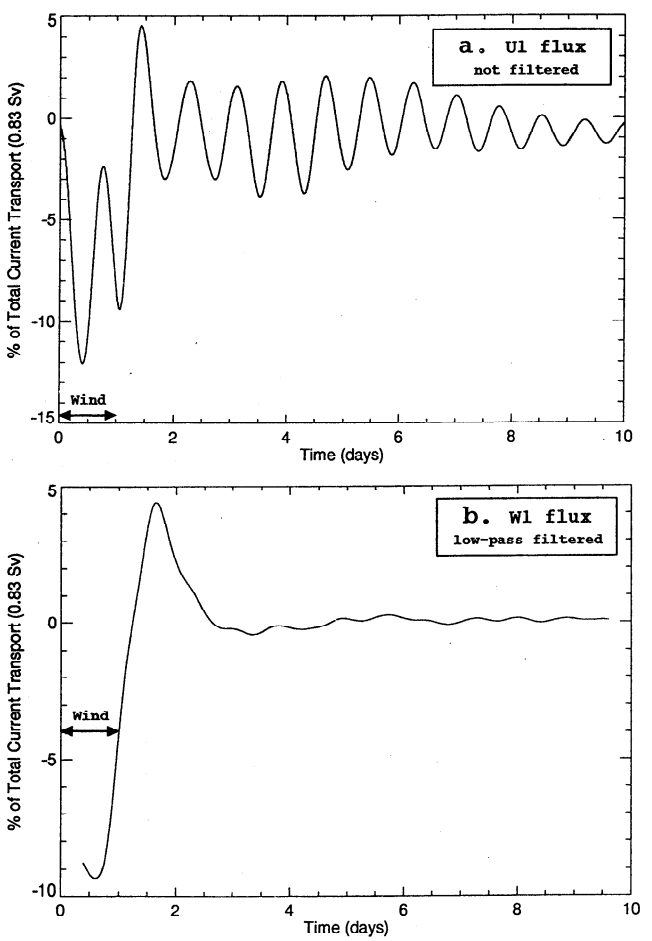

Figure 8. Time evolution of fluxes in the canyon box during and after the outbreak of an easterly wind burst (experiment WE-SL); fluxes are expressed as a ratio to the total along-shore transport (1 Sv in this configuration): (a) Net cross-shore flux through the offshore side of the box in the upper 50 m (U_1, counted positive offshore) and (b) net vertical flux through the horizontal plane at 50-m depth (W_1, counted positive upward). The latter time series has been low-pass filtered to remove inertial oscillations.

Table 2. Extrema Values of the Cross-Shore and Vertical Fluxes with Configuration SL

Fluxes	Experiment S-SL	WE-SL	WN-SL
Upstream Box			
min(U_1)	-0.1	-1.0	-1.3
max(U_1)	-0.08	0.4	1.5
Canyon Box			
min(U_1)	-0.58	-6.4	-4.5
max(U_1)	-0.54	1.8	5.4
min(U^-_{tot})	-2.0	-7.5	-10.0
max(U^+_{tot})	0.8	7.3	13.3
min(W_1)	0.05	-6.9	-10.7
max(W_1)	0.11	4.7	9.2

See text in section 3.3 and Figure 4: In experiment S, the 10-day period is considered when the flow is quasi-stationary while in wind-forced experiments WE and WN, the 10-day period starts at the outbreak of the wind. Fluxes are expressed as a ratio to the total along-slope inflow ($V_{tot} = V_{shelf} + V_{rmslope}$) which is 0.8 Sv in configuration SL. U_1 is the net cross-shore flux in the upper layer through the offshore side of the boxes and U^-_{tot} and U^+_{tot} are the total onshore and offshore fluxes, respectively, integrated from surface to bottom at the same place ($\sum_i U_i = U^-_{tot} + U^+_{tot}$). W_1 is the vertical flux through the horizontal plane at 50-m depth. All fluxes reported in this table are counted positively when directed offshore or upward and negatively when directed onshore or downward.

The modeled oscillations are essentially baroclinic, and the offshore boundary condition certainly affects them, but they are a physical feature of the model and have been observed in other canyons (X. Durrieu de Madron, personal communication, 1998). However, the most interesting observation in Figure 8a is the onshore (negative) transport in the surface layer (U_1) during the wind event. While the wind keeps blowing, this onshore flux peaks at 12% of the total along-slope transport. This horizontal cross-slope flow is associated with significant vertical motions, as shown by the time series of W_1, the vertical flux through the horizontal plane at 50-m depth (Figure 8b) (Note that this time series has been low-pass filtered to remove inertial oscillations and highlight the low-frequency motions. Otherwise it would look much like Figure 8a). Meanwhile, cross-slope fluxes remain comparatively weak in areas upstream and downstream of the canyon, remaining below 2% of the along-slope transport (Table 2). Therefore the canyon clearly appears to enhance cross-slope and vertical exchanges.

Lagrangian calculations show that although the wind burst drastically modifies the instantaneous circulation pattern in the canyon, it is neither long nor strong enough to renew the waters previously trapped in the steady anticyclonic eddy (Figure 9a). Eddy waters are

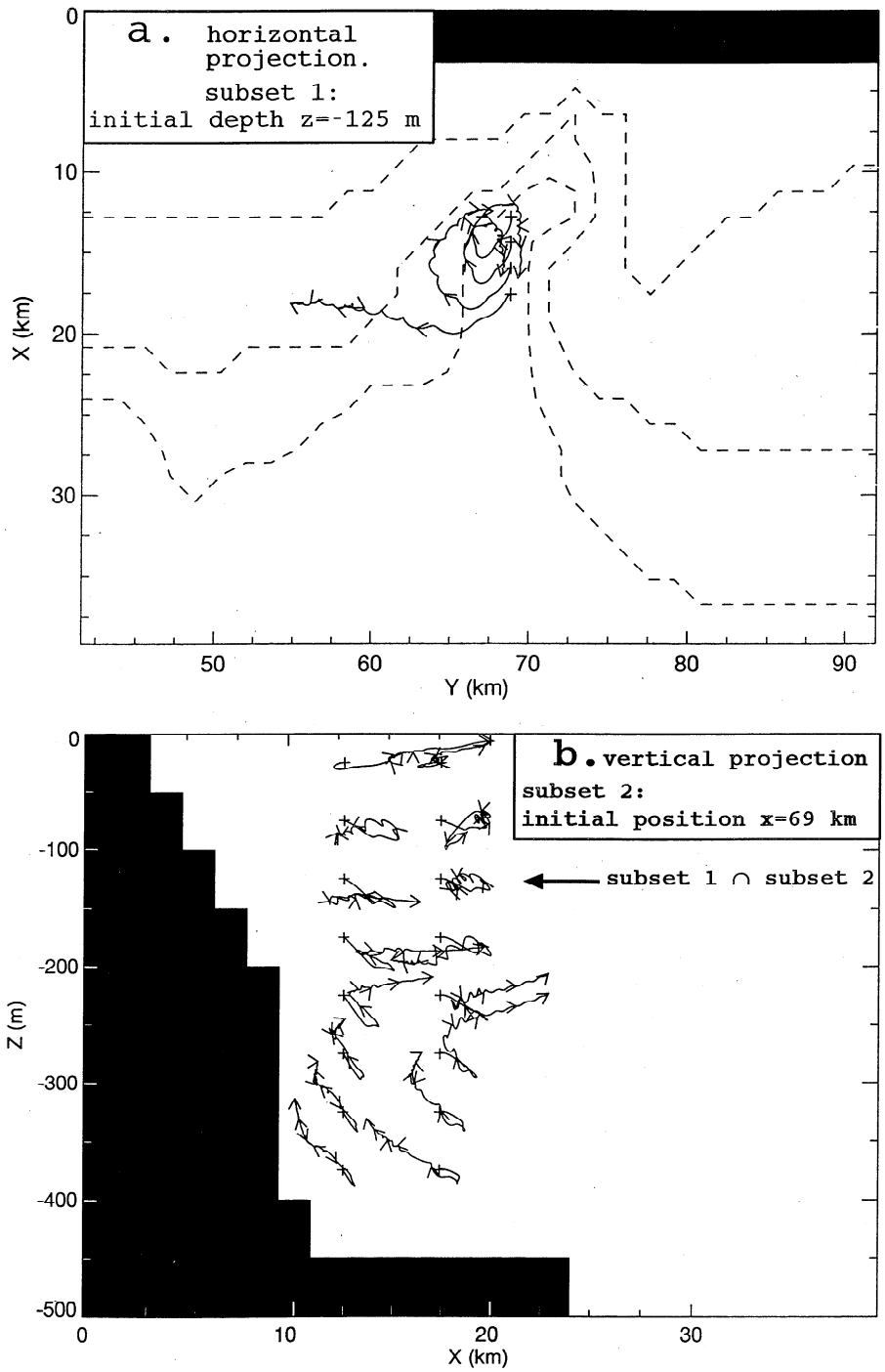

Figure 9. Circulation induced by an easterly wind burst (experiment WE-SL): 10-day trajectories of the drifters released at the outbreak of the wind at y_0=69 km within the canyon. The initial positions are represented by crosses, and arrows are plotted every 2 days to show the direction of the movement. (a) Horizontal projection of the trajectories of all drifters released at 125-m depth (subset 1). Bottom topography is indicated with dashed lines. (b) Vertical projection in a cross-shore plane (looking upstream) of a sample of trajectories (subset 2).

downwelled by about 30 m in the first 12 hours and reach a zone sheltered by the canyon walls, where velocities are lower (Figure 9b). As a result, they do not drift away and remain within the canyon. Nevertheless, the trajectory of one water parcel advected downstream indicates that part of the water located at the periphery of the eddy may be mixed out (Figure 9a).

As the wind relaxes, the vertical motion is inverted, leading to an important upwelling event which reaches its maximum 6 hours after the wind stops (Figure 8b). In the surface layer an anticyclonic eddy develops close to the head of the canyon, and the dense waters pumped in the middle of the shelf force a geostrophic current reversal along the coast (Figure 10). The surface eddy

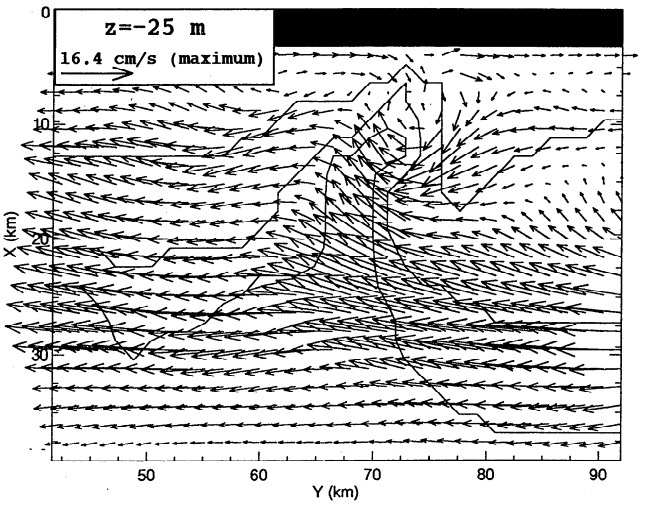

Figure 10. Circulation induced by an easterly wind burst (experiment WE-SL): map of horizontal velocity at surface in the canyon 1 day after the wind stops. The 100-, 200-, and 400-m isobaths are plotted with solid lines.

is still present, though weakened, 9 days after the wind burst while the deeper steady eddy is already restored to its initial state (Figures 5c and 5d). Trajectories show that the effect of the upwelling is almost as strong as that of the previous downwelling. After moving downward during the 1-day wind event, all drifters ascend back during another about 1-day period (up to the first arrow in Figure 9b). The time evolution during the following days is characterized by the reformation of the steady vertical cell in the 200- to 500-m layer. On the whole, the relaxation to the steady state is slower for the very coastal circulation than for the offshore deep layers. It is likely that perturbations in the 100- to 500-m depth range within the canyon are more rapidly swept out because this layer is directly fed by the along-slope current through the mouth of the canyon. Besides, no significant residual flow is observed after the wind event: The circulation within the canyon relaxes back to its initial steady state.

Experiment WE-SH shows that the offshore location of the along-slope current only influences the magnitude of the upwelling and downwelling, while the general patterns of the flow oscillation due to the wind are not affected. In experiment WE-SH, however, there remains a weak anticyclonic circulation within the canyon throughout the wind burst. The general trend is that in WE-SH the wind effect on the steady circulation is not so marked as in WE-SL. As a matter of fact, cross-shelf fluxes are smaller in WE-SH than in WE-SL. This difference may be explained by the fact that advection from the upstream boundary is faster in the region of highest variability (the canyon) when the current is centered on the outer shelf (SH configuration).

5.2. Response to a Northerly Wind Burst (Experiments WN)

The only difference between the settings of experiments WE described above and those of experiments WN described below is the wind direction, which is rotated by 90°. Therefore the wind is now normal to the coast and blows offshore from the north. We mainly focus on the results given by configuration SL (WN-SL experiment).

The northerly wind produces an oscillation of the flow which is opposite to that triggered by the easterly wind. This time, an intense upwelling occurs during the wind burst followed by a downwelling as the wind relaxes. The upwelling is at a maximum 12 hours after the outbreak of the wind, and it is associated with a strong anticyclonic eddy which forms in the upper layers of the canyon. This eddy is similar to the one observed during the relaxation of the flow (upwelling phase) after the easterly wind burst (Figure 10). In the surface layer the eddy lies over the canyon head and exhibits a maximum relative vorticity of $0.6f$ (Figure 11a), while, at greater depths, it is located slightly offshore and centered at the mouth of the canyon (Figures 11b and 11c). This eddy drives the flow onto the upstream canyon wall and forces upward motions. This process, however, is restricted to the interior of the canyon, while, outside, the flow is directed offshore near the slope.

Below 300 m an overall reversal of the along-slope circulation is observed (Figure 11d). It corresponds to an eastward barotropic flow produced by the increase of the surface elevation, as waters are pushed away from the coast by the wind. This barotropic current, which involves velocities less than 5 cm s^{-1}, is able to reverse the westward along-slope density-driven flow below 300 m only. As a result, the flow in the canyon impinges onto the eastern flank of the canyon and is redirected toward its head. Vertical velocities associated with this process are observed to be as large as 40 m d^{-1}. The intense flow directed onto the canyon flank at all depths below 50 m produces upwelling and a shrinking of the water column. Since potential vorticity has to be conserved, anticyclonic relative vorticity is generated, which probably is responsible for the anticylonic eddy observed in the upper layers. However, a question can be raised about why, if the argument of potential vorticity is valid, a cyclonic eddy is not obtained in the WE experiments as the flow is directed offshore in the canyon (see section 5.1 and Figures 7b-7d). The reason for this lack of symmetry in the wind-induced flow pattern may be that the canyon is located at the right side of the along-slope current, which is characterized by a strong anticyclonic shear vorticity. Hence the current provides a source of negative vorticity for the enhancement of the anticyclonic eddy in experiments WN, whereas it cancels out the generation of cyclonic vorticity in experiments WE.

The 10-day trajectories, beginning at the outbreak of the wind, indicate that drifters released in the closed

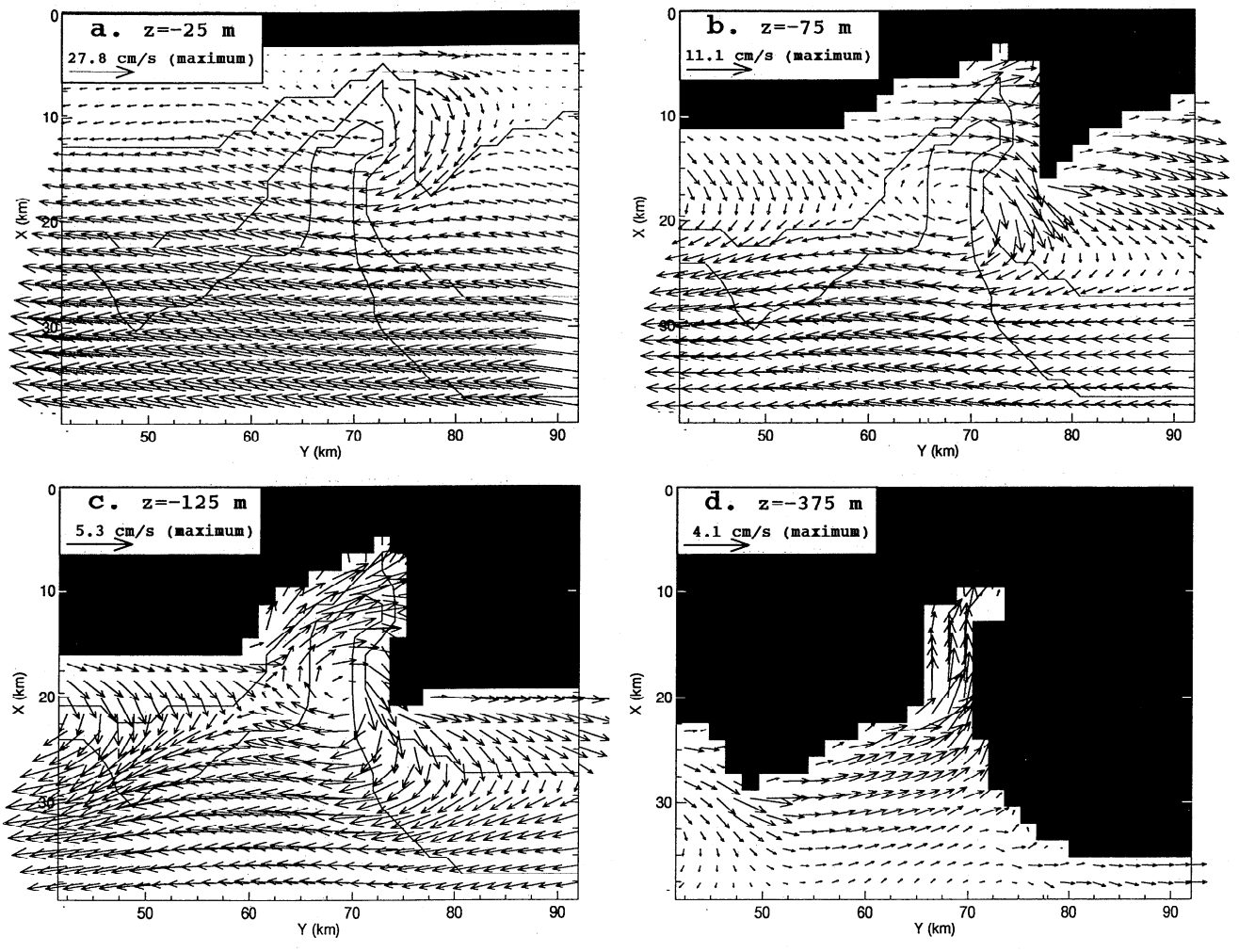

Figure 11. Circulation induced by a northerly wind burst (experiment WN-SL): maps of horizontal velocity in the canyon at four representative depths 12 hours after the wind starts. The 100-, 200-, and 400-m isobaths are plotted with solid lines.

steady eddy between 100 and 200 m, including subset 1, are able to exit the canyon (Figure 12a). This outflow of canyon waters can be attributed to the strength of the upwelling (as large as 50 m d^{-1}, that is, 6 times larger than without wind), which shifts canyon subsurface waters to upper layers, where they are entrained by the large horizontal flow (Figure 12b). As a matter of fact, the vertical residual displacement of water parcels in the canyon is generally upward. The density field in the upper layer shows that dense waters, normally found at 60-m depth in the steady state circulation, do reach the surface at the canyon head (Figure 13), bearing evidence of the particular role of the canyon head in enhancing upwelling. Thus a northerly wind (upwelling favorable) allows canyon waters to be flushed away (Figure 12a), which is not the case with an easterly wind (downwelling favorable) of the same intensity and duration (Figure 9a).

The importance of the upwelling in the canyon can be quantitatively estimated from time series of fluxes in the canyon box (Figure 14), which appear to be concentrated in the upper 50 m (Table 2). As in experiments WE, inertial waves are generated during the wind burst. After wind relaxation they are slowly damped and the intense upwelling is followed by a downwelling, the maximum of which is even larger than that of the upwelling (Figure 14). The offshore transport U^{+}_{tot} and onshore transport U^{-}_{tot} at the mouth of the canyon peak at 13% and 10%, respectively, of the along-slope transport, while the upward vertical flux at 50 m (W_1) reaches 9%.

Results are fairly similar with configuration SH. However, the response to the wind is again slightly weaker (cross-shelf fluxes are typically 30% less) than it is in experiments WE.

6. Discussion

6.1. Sensitivity Analyses

We first report results of several sensitivity analyses concerning the representation of topography in the model. Experiments similar to experiments S performed using a higher vertical resolution (20 layers 25 m thick

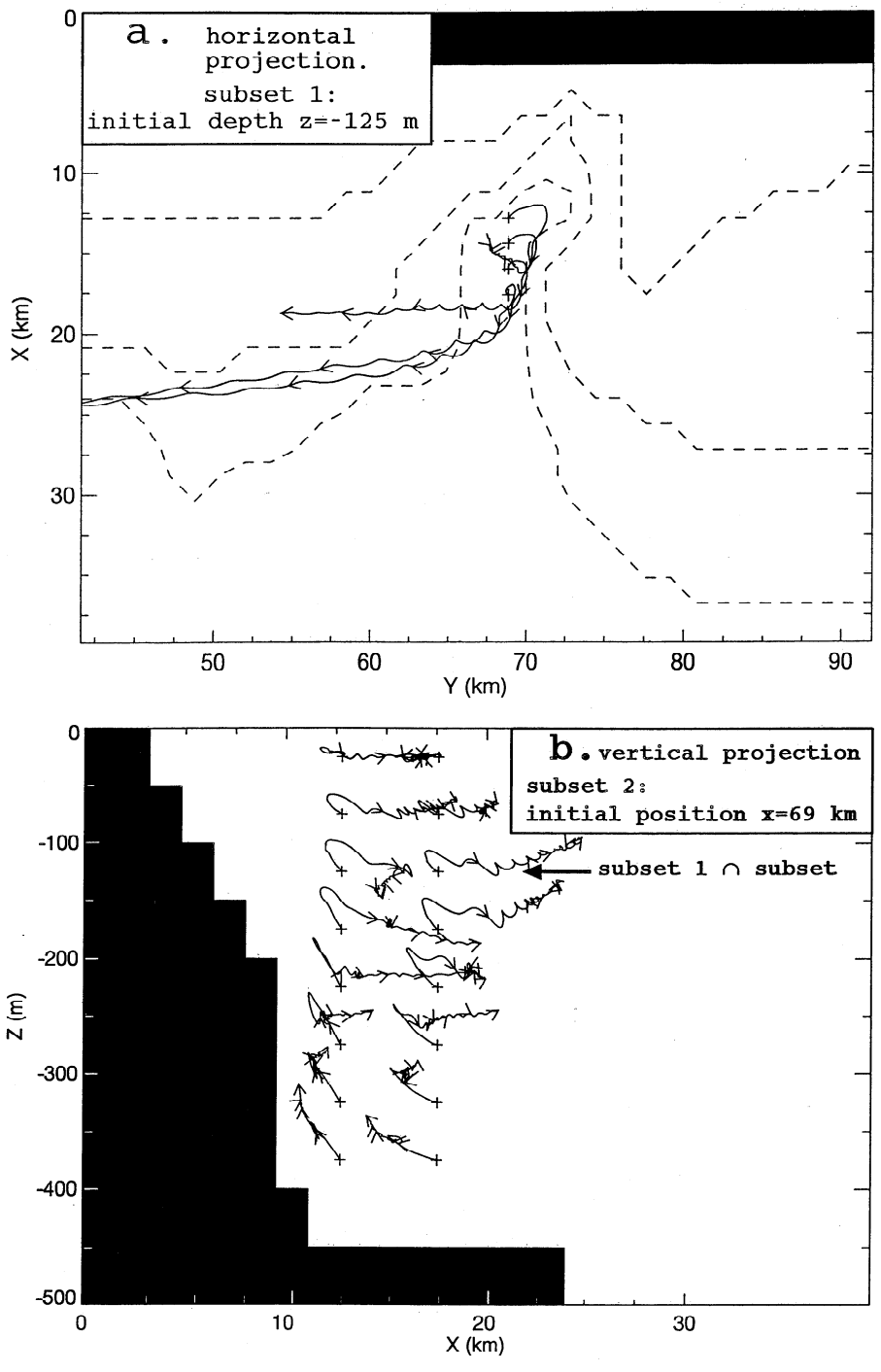

Figure 12. Circulation induced by a northerly wind burst (experiment WN-SL): 10-day trajectories of the drifters released at the outbreak of the wind at y_0=69 km within the canyon. The initial positions are represented by crosses, and arrows are plotted every 2 days to show the direction of the movement. (a) Horizontal projection of the trajectories of all drifters released at 125-m depth (subset 1). Bottom topography is indicated with dashed lines. (b) Vertical projection in a cross-shore plane (looking upstream) of a sample of trajectories (subset 2).

instead of 10 layers 50 m thick) do not evidence any important difference in the flow pattern. Experiments using a higher horizontal resolution (1.2 km instead of 1.6 km) also do not reveal important changes. Nevertheless, as the coastline is not straight, high-resolution experiments modify some details of the flow, but these are irrelevant to the main circulation patterns. A simulation done with a deeper bottom depth (1050 m instead of 500 m) provides interesting results which shed light on the role of the canyon geometry in shaping the flow pattern. In this simulation a second anticyclonic eddy is present in deeper layers where the canyon is wider (below 800 m), which is below the bottom of our reference model and offshore of the slope of our reference

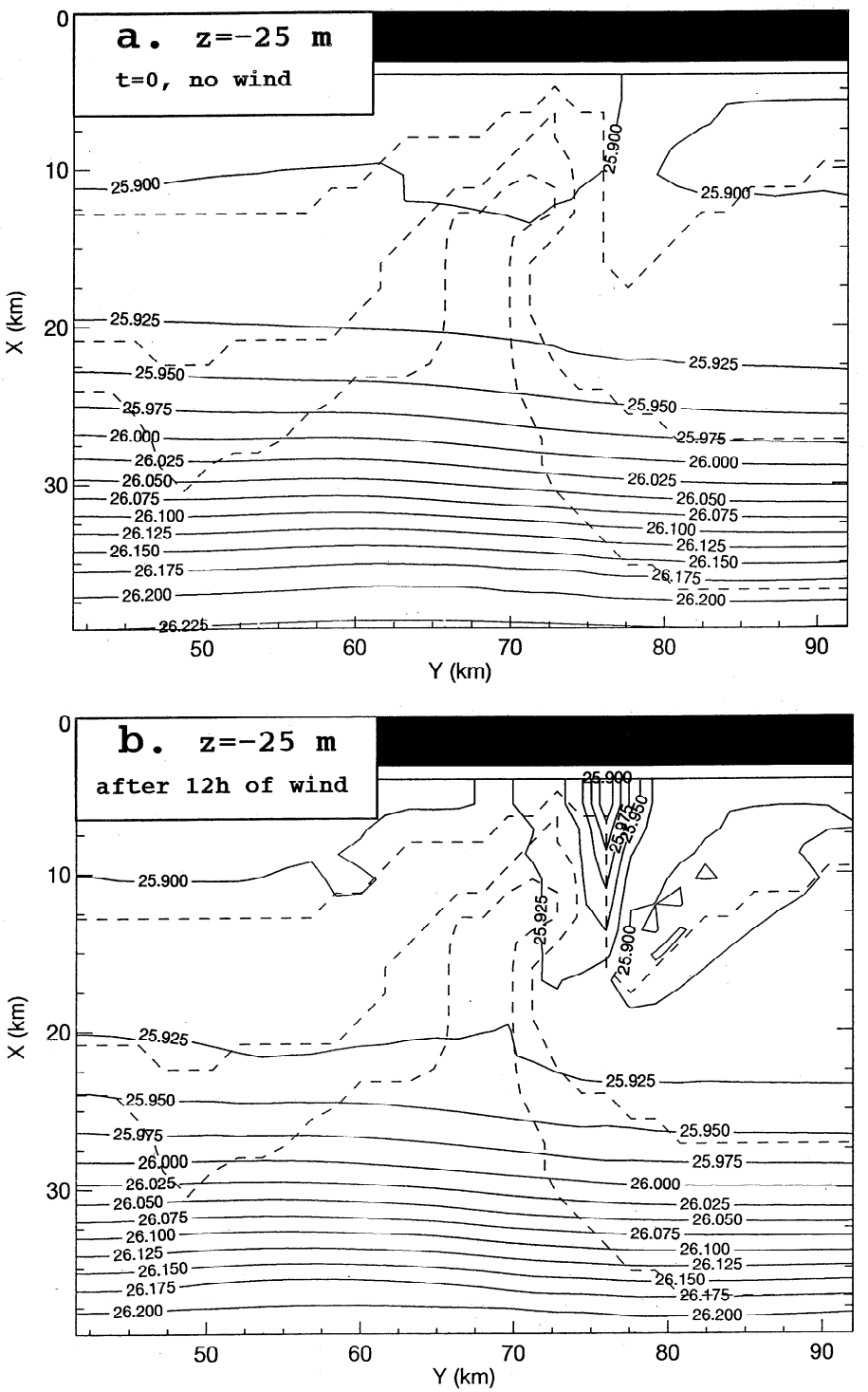

Figure 13. WN-SL experiment: density field in the surface layer (a) before the northerly wind starts (steady state circulation) and (b) 12 hours after the outbreak of the wind. Bottom topography is indicated with dashed lines.

model. This deeper flow does not apparently interact with the flow above 600 m, which gives support to our initial depth limit at 500 m.

With the parameters of our main experiments, eddies do not exist where the canyon is narrower than 4 km because the ageostrophic flow is important and essentially cross-shore. This is confirmed by a simulation done with an idealized Gaussian canyon, 8 km wide at all depths, which shows that no vertical cell develops, while an anticyclonic eddy generally appears at all depths. This latter simulation also indicates that the vertical cell is not necessary for the eddy to form and confirms momentum diffusion as the main mechanism maintaining the eddy; this is also supported by the absence of an isopicnic dome, mentioned in section 4, in experiment S-SL. However, if in the Gaussian canyon the curvature

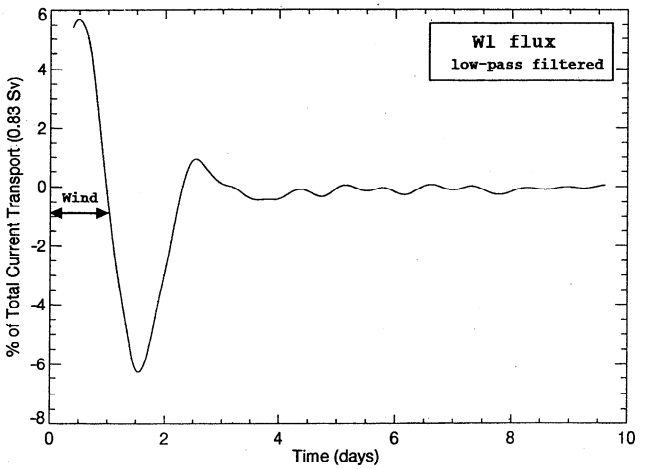

Figure 14. Time evolution of the net vertical flux through the horizontal plane at 50-m depth (W_1, counted positive upward) in the canyon box during and after the outbreak of a northerly wind burst (experiment WN-SL). Fluxes are expressed as a ratio to the total along-shore transport (1 Sv in this configuration). This time series has been low-pass filtered to remove inertial oscillations.

of isobaths at the intersection of the canyon walls with the slope is smooth, the flow meanders in the canyon instead of forming an eddy inside the canyon. This shows that canyon waters need to be sheltered, to some extent, in order to allow the formation of an eddy. No single clear parameter has yet emerged to determine the boundary between these two types of flow, but important parameters are the surface and intermediate stratification and geometrical characteristics of the canyon like its width and upstream curvature.

The shelf and the bottom boundary layer are, in principle, places where the higher resolution offered by a sigma coordinate (following the topography) in the vertical would be relevant to gain accuracy in the simulations. However, sensitivity experiments performed with our z Cartesian coordinate model by increasing the resolution over the shelf (five layers in the upper 50 m) do not present any important change in the circulation. Also, halving or doubling the bottom drag coefficient proves to have very little impact. As an example, the only noticeable difference in the latter case is that the flow on the shelf is reduced by 20%, while the qualitative pattern remains the same and the current still crosses the canyon perpendicularly to its axis in the upper 50 m. As the modeling of the flow in both critical areas, the shelf and the bottom boundary layer, does not appear to be significantly modified by increasing the vertical resolution, we believe that the model z coordinate is adequate and need not be replaced by a sigma coordinate. The latter presents several drawbacks such as the bias involved in the computation of the pressure gradient over steep topography and the introduction of an artificial vertical diffusion.

Eventually, the boundary conditions used in this study need a brief justification. Although presenting several difficulties, fully open boundary conditions seem to us an adequate and relevant choice for the problem we deal with. Sensitivity tests performed using the same model with periodic boundary conditions show that perturbations generated past the canyon increase the complexity of the flow adjustment in the canyon if they are reinjected upstream. This would be closer to reality, indeed, but it makes too difficult the interpretation of the results. In this case, the model should include a large buffer zone to damp the perturbations and also an an artificial nudging term to counteract dissipation within the along-slope flow as done by *Haidvogel et al.* [1991].

6.2. Comparison With Data and Previous Models

A description of the time and space variability of the surface flow in Blanes Canyon, derived from satellite imagery, is given by *Masó et al.* [1990]. They find that in 15 images (out of 43), the surface current crosses the isobaths without any appreciable deflection, as in our experiments S (Figure 5a). In the remaining 28 images the flow is distorted by the canyon, and these distortions could be ascribed to wind events, like our experiments WN and WE, or to density anomalies lying over the shelf. In situ measurements obtained with a ship-mounted acoustic doppler current profiler (ADCP) in the area of Blanes Canyon in June 1993 are reported by *Rojas et al.* [1995]. These data show that over the shelf, the flow is reversed (flowing to the east) above the thermocline (approximately, the upper 50 m), because of pools of fresh water of northern continental origin. Below the thermocline, at 73-m depth, the flow crosses the isobaths above the canyon, and a weak anticylonic eddy can be appreciated at the head of the canyon, forming an overall flow pattern similar to the result of our S-SH experiment (Figure 5b). Unfortunately, ADCP data at greater depths are not reported. Recent works on Blanes Canyon include field studies of particle transport in the canyon by T. Granata et al. (Hydrodynamics and particle transport associated with a submarine canyon off Blanes, submitted to *Journal of Marine Research*, 1998), which show that waters in the canyon are quite isolated from the offshore slope current, but they also suggest strong downwelling, which could be ascribed to easterly winds. Unfortunately, neither of these studies explicitly treats the effect of wind forcing, which makes difficult any discussion of our wind-forced experiments.

In situ observations collected in other canyons of the world ocean support some of our results. Early field studies carried out on the northeastern U.S. coast by *Kinsella et al.* [1987] on Carson Canyon, by *Hunkins* [1988] on Baltimore Canyon, and by *Noble and Butman* [1989] on Lyndonia Canyon give evidence of waters flowing straight across the canyons and strong disruptions, not in the last case, of this circulation by winds. It

is interesting to note that these canyons, as is Blanes Canyon, are situated on the path of a current driven by a density front. Nevertheless, many authors give no clue to the deep circulation in the canyons. The most comprehensive data set concerning canyons, including current-meter, conductivity-temperature-depth (CTD), and nephelometric measurements, was collected in Astoria Canyon [*Hickey*, 1997]. The Astoria Canyon depth (600 m) and width (7 km) and the mean Brunt-Väisälä frequency in the area ($5\text{-}10 \times 10^{-3}\,s^{-1}$) are quite similar to those of Blanes Canyon. However, the shelf is slightly deeper in the vicinity of Astoria Canyon, while the along-shore circulation (maximum current of $\sim 20\ cm\,s^{-1}$) is driven by local and/or remote winds. *Hickey* [1997] reports that above the canyon, the current crosses the isobaths in the upper 50 m whatever the wind strength is, while it is slightly deviated toward the coast between 50 m and the canyon rim (150 m) in low-wind conditions. She also documents a fully three-dimensional circulation in the canyon and the formation of a cyclonic eddy at intermediate depths when the wind is relatively low. Our model results present important analogies with these observations if we take into account that the mean current in our model flows with the coast on its right, that is, in the opposite way to the mean flow over Astoria Canyon. Hence the anticyclonic eddy obtained in experiment S would correspond to the cyclonic eddy described by *Hickey* [1997], and both could be explained by the same dynamics. When the wind, blowing with the coast on its left (upwelling favorable), reaches its maximum, the eddy in Astoria Canyon is disrupted by a massive subsurface onshore flux, and an important rebound downwelling occurs after wind relaxation. Both observations seem to be reproduced in experiment WN. Many circulation patterns observed in Astoria Canyon can be interpreted in terms of vorticity dynamics, as shown by the good correlation existing between stretching vorticity and relative vorticity. However, this correlation particularly decreases when the wind is low (less than $5\ m\,s^{-1}$), suggesting that other processes, such as diffusion of momentum, may account for the driving of the canyon eddy. Eventually, the upwelling cell modeled in our experiments is akin to the topographic upwelling described at the head of a canyon located near Vancouver Island by *Freeland and Denman* [1982]. The authors explain that the observed upwelling is due to the acceleration of the flow by the along-canyon pressure gradient, while the Coriolis force is small because the canyon is very narrow. This is also the reason given by *Noble and Butman* [1989] for the along-canyon flow observed in Lydonia Canyon. As we detailed it in section 4, this kind of argument can apply only to the part of Blanes Canyon which is below 200-m depth, where the canyon is very narrow. However, in our case the driving pressure gradient is directed toward the shore, accelerating the flow in the offshore direction. It is interesting to note that this phenomenon also yields an upwelling, which does not reach the surface in Blanes Canyon, while the driving force is in the opposite direction of the case observed by *Freeland and Denman* [1982]. Besides, in our model the pressure gradient is still largely balanced by the Coriolis force. It is to be expected that the degree of ageostrophism is higher in the real canyon, where it is narrower than the resolution of our grid.

The analysis of our results with regard to previous numerical studies deserves attention too. As indicated by our experiments, stratification, nonlinear terms, and complex canyon topography play a major role in shaping the specific features of the steady canyon circulation: cross-isobath flows, diffusive eddies, and upwelling cells. The importance of stratification is demonstrated by the results of *Rojas et al.* [1995], who fail in reproducing their observations with a finite element model solving the steady state shallow-water equations in a homogeneous (not stratified) ocean. The flow in their model systematically follows the isobaths, unlike the real flow measured in situ. We have carried out several experiments to check the sensitivity of our model to the strength of stratification. The results show that when stratification is weak, the flow is aligned with the isobaths at all depths, confirming the flow modeled by *Rojas et al.* [1995]. Hence stratification is essential for models to reproduce cross-isobath flows over canyons. Besides, ageostrophic terms are needed to maintain the steady eddy in the canyon. This probably explains why other models lacking stratification [*Klinck*, 1988] and models of geostrophic adjustment [e.g., *Klinck*, 1989] miss these features.

Two recent studies, including more complex dynamics, are worth mentioning. *Allen* [1996] investigates the wind-induced circulation in several canyons with a model including nonlinearities and stratification. The effect of an upwelling favorable wind forcing is modeled by a water sink within a coastal strip where volume does not have to be conserved. Hence there is no surface Ekman transport but only a weak onshore flow in the deep and intermediate layers. This makes difficult the comparison between our results and hers. Nevertheless, one of Allen's experiment simulating a wind burst in a very narrow canyon (her Run 6 in Figures 11a and 11b) shares some features with our WN experiments (Figure 11a): In both experiments, strong upwelling and anticyclonic vorticity are produced at the very head of the canyon.

Klinck [1996] uses a primitive equations semispectral model to assess the relative importance of two essential factors: stratification and along-shore flow direction. Modeling flows in a Gaussian-shaped canyon, he concludes that flow direction governs the shape of vertical and cross-slope motions, while stratification determines their magnitude. He also obtains a surface flow that ignores bottom topography if stratification is enhanced, but no eddy or vertical cell forms in the canyon. A detailed comparison between his results and ours is made difficult by the difference in the model set-

tings. First, Klinck's model is periodic and forced by a stream function prescribed at the coast and at the offshore boundary. This stream function is equivalent to an external cross-shore pressure gradient uniform over the whole model domain. This pressure gradient, as stated by the author, governs the acceleration of the current in the canyon and strongly controls the model solution. Hence, in Klinck's experiments dealing with an along-slope circulation bounded by the coast on its right, the flow is constrained to follow the isobaths over the canyon. On the contrary, as the forcing in our model is restricted to the upstream boundary, the flow is allowed to freely evolve in the domain. As a matter of fact, the pressure gradient in the canyon is weak in our model. Second, the velocity field in Klinck's model is almost uniform at all depths in his whole domain (low vertical and horizontal shears), and, as a consequence, the adjustment has a strong barotropic character. In our model the strong current shear in the horizontal and vertical allows a more complex equilibrium to establish. In order to confirm this diagnostic, we have run our model with a Gaussian canyon similar to Klinck's. If the prescribed inflow is barotropic, the adjustment over the canyon also is barotropic and the flow follows the isobaths as done by *Klinck* [1996]. However, if a baroclinic inflow is imposed, an eddy forms in the canyon, which shows that the structure of the along-slope flow is crucial for the dynamics in the canyon.

7. Conclusions

The numerical results described in this paper suggest that the baroclinic along-slope flow impinging onto the steep and narrow Blanes Canyon off the Catalan coast forces a fully three-dimensional circulation in the interior of the canyon. Three different patterns can be identified in the vertical. Above the canyon rim (approximately, the upper 50 m), the flow crosses the isobaths and is hardly deflected toward the coast over the upstream wall of the canyon. This behavior can be attributed to the strong stratification in the upper layers which disconnects the flow from the underlying bottom. The circulation in the upper (and wider) part of the canyon ($\sim$ 100-200 m) is characterized by an anticyclonic eddy which seems to be produced by momentum diffusion from the along-slope current through the mouth of the canyon. This eddy develops in the lee of the upstream canyon wall which shelters canyon waters from the offshore energetic flow in an area of weak pressure gradients. In the deeper (and narrower) part of the canyon ($\sim$ 200-500 m), right beneath the eddy, a vertical cell upwells offshore deep waters over the bottom slope toward the canyon head. This upward motion accelerates the anticyclonic rotation at the base of the eddy. A sensitivity analysis shows that when the surface is stratified, the flow pattern can be directly related to the shape of the canyon at various depths. Eddies tend to develop where canyons are wide and make a sharp angle with the shelf-break, whereas vertical cells appear only where canyons are narrow. However, if the along-slope circulation is barotropic, the flow simply follows the isobaths at all depths.

The variability of the offshore position of the along-slope current axis may have an impact on the adjustment of the flow in the canyon, as the orientation of the current with respect to the canyon changes, and this effect needs to be investigated. From the present study we can conclude that the offshore position of the current does not qualitatively influence the pattern of the flow in the canyon, while it changes its intensity. However, moderate gusts of wind drastically modify the circulation and intensify cross-shore and vertical motions. This ageostrophic circulation is substantially amplified in the canyon, where the flow pattern presents large-amplitude oscillations characterized by a downwelling (upwelling) during the easterly (northerly) wind burst followed by a rebound upwelling (downwelling) as the wind relaxes. The enhanced vertical exchange in the canyon appears to be 4-6 times larger than outside the canyon. The upwelling induced by the northerly wind burst is capable of flushing waters trapped in the canyon eddy and can supply nutrients to the euphotic layer.

Sensitivity experiments show that the cross-isobath flow modeled at surface and the canyon eddy are robust features hardly altered by changes of model parameters and resolution. Furthermore, they are corroborated by observations collected in Blanes Canyon [*Rojas et al.*, 1995] and present high similarities with the description of the flow pattern in Astoria Canyon [*Hickey*, 1997]. Also, the canyon eddy could account for the isolation of waters observed in the interior of Blanes Canyon from measurements of particle transports. This trapping of waters may have a strong impact on the biomass distribution as stability of physical properties within closed eddies are a determinant factor for larvae isolation and enhanced species reproduction. Besides, the high nutrient input produced by permanent or sporadic upwellings may favor the increase of biomass, thereby helping the farming of mussels on the inner shelf, downstream of the canyon.

Acknowledgments. This work is a contribution to the MATER project (MAS3-CT96-0051) funded by the European Community (DG XII) MAST program. Partial support from CICYT (AMB95-0901CO2-01 and MAR95-1861) is also acknowledged as well as support from Ecole Polytechnique, the French Délegation Générale pour l'Armement and Service Hydrographique et Océanographique de la Marine. We are thankful to Miquel Canals (Universitat de Barcelona, Spain) for providing the bathymetric data set and to X. Durrieu de Madron (CEFREM, Université de Perpignan, France) for sharing his views and data on canyons. R.L. Haney (Naval Postgraduate School, Monterey, CA) and anonymous reviewers made relevant comments which were very useful in improving the manuscript.

References

Allen, S., Topographically generated, subinertial flows within a finite length canyon, *J. Phys. Oceanogr., 26*, 1608–1632, 1996.

Álvarez, A., J. Tintoré, and A. Sabatés, Flow modification and shelf-slope exchange induced by a submarine canyon off the northeast Spanish coast, *J. Geophys. Res., 101*, 12,043–12,055, 1996.

Canals, M., J. Serra, and O. Riba, Toponimia de la Mar Catalano-Balear, *Boll. Soc. Hist. Nat. Balears, 26*, 169–194, 1982.

Church, T.M., C.N.K. Mooers, and A.D. Voorhis, Exchange processes over a middle Atlantic bight shelfbreak canyon, *Estuarine Coastal Shelf Sci., 19*, 393–411, 1984.

Font, J., J. Salat, and J. Tintoré, Permanent features of the circulation in the Catalan Sea, in *Océanographie pélagique méditerranéenne*, edited by H.J. Minas and P. Nival, *Oceanol. Acta, 11*, Special Issue, 51–57, 1988.

Freeland, M.J., and K.L. Denman, A topographically controlled upwelling center off southern Vancouver Island, *J. Mar. Res., 40*, 1069–1093, 1982.

García-Ladona, E., A. Castellon, J. Font, and J. Tintoré, The Balearic current and volume transports in the Balearic basin, *Oceanol. Acta, 19*, 489–497, 1996.

Haidvogel, D.B., A. Beckmann, and K.S. Hedstrom, Dynamical simulations of filament formation and evolution in the coastal transition zone, *J. Geophys. Res., 96*, 15,017–15,040, 1991.

Hickey, B., Coastal submarine canyons, paper presented at 'Aha Huliko' A Workshop on Flow Topography Interactions, Off. of Nav. Res., Honolulu, 1995.

Hickey, B., The response of a steep-sided, narrow canyon to time-variable wind forcing, *J. Phys. Oceanogr., 27*, 697–726, 1997.

Hunkins, K., Mean and tidal currents in Baltimore Canyon, *J. Geophys. Res., 93*, 6917–6929, 1988.

Kinsella, E.D., A.E. Hay, and W.W. Denner, Wind and topographic effects on the Labrador current at Carson Canyon, *J. Geophys. Res., 92*, 10,853–10,869, 1987.

Klinck, J.M., The influence of a narrow transverse canyon on initially geostrophic flow, *J. Geophys. Res., 93*, 509–515, 1988.

Klinck, J.M., Geostrophic adjustment over submarine canyons, *J. Geophys. Res., 94*, 6133–6144, 1989.

Klinck, J.M., Circulation near submarine canyons: A modeling study, *J. Geophys. Res., 101*, 1211–1223, 1996.

La Violette, P.E., J. Tintoré, and J. Font, The surface circulation of the Balearic Sea, *J. Geophys. Res., 95*, 1559–1568, 1990.

Masó, M., P.E. La Violette, and J. Tintoré, Coastal flow modification by submarine canyons along the NE Spanish coast, *Sci. Mar., 54*, 343–348, 1990.

Millot, C., Circulation in the western Mediterranean Sea, *Oceanol. Acta, 10*, 143–149, 1987.

Monhagan, J.J., Particle methods for hydrodynamics, *Comput. Phys. Rep., 3*, 71–124, 1985.

Munk, W., and E.R. Anderson, Notes on a theory of the thermocline, *J. Mar. Res., 7*, 276–295, 1948.

Noble, M., and B. Butman, The structure of subtidal currents within and around Lydonia Canyon: Evidence for enhanced cross-shelf fluctuation over the mouth of the canyon, *J. Geophys. Res., 94*, 8091–8110, 1989.

Orlanski, I., A simple boundary condition for unbounded hyperbolic flows, *J. Comput. Phys., 21*, 251–269, 1976.

Petruncio, E.T., Observation and modeling of the internal tide in a submarine canyon, Ph.D. dissertation, 181 pp., Nav. Postgrad. School, Monterey, Calif., 1996.

Press, W.H., S.A. Teukolsky, W.T. Vetterling, and B.P. Flannery, *Numerical Recipes*, 818 pp., Cambridge Univ. Press, New York, 1992.

Rojas, P., et al., On the structure of the mean flow in the Blanes canyon area (NW Mediterranean) during summer, *Oceanol. Acta, 18*, 443–454, 1995.

Tintoré, J., D.P. Wang, E. García, and A. Viúdez, Near-inertial motions in the coastal ocean, *J. Mar. Sys., 6*, 301–312, 1995.

Wang, D.P., Development of a three-dimensional limited-area (island) shelf circulation model, *J. Phys. Oceanogr., 12*, 605–616, 1982.

Wang, D.P., Effects of small-scale wind on coastal upwelling with application to Point Conception, *J. Geophys. Res., 102*, 15,555–15,566, 1997.

F. Ardhuin, Department of Oceanography, Naval Postgraduate School, 833 Dyer Road, Monterey, 93943-5122, CA (e-mail: ardhuin@met.nps.navy.mil)

J.M. Pinot, EPSHOM/CMO, 13 rue du Chatellier, 29275 Brest, France (e-mail: jmichel@shom.fr)

J. Tintoré, Institut Mediterrani d'Estudis Avançats, Universitat de les Illes Balears, 07071 Palma de Mallorca, Spain (e-mail: dfsjts0@ps.uib.es)

(Received February 13, 1998; revised December 18, 1998; accepted January 25, 1999.)